

# Numerical study on filtration law of supercritical carbon dioxide fracturing in shale gas reservoirs

Zhifeng Luo, Lin Wu, Liqiang Zhao  and Nanlin Zhang, State Key Laboratory of Reservoir Geology and Development Engineering, Southwest Petroleum University, Chengdu, China

Weihua Chen, Engineering Technology Research Institute of Southwest Oil & Gas Field Company, PetroChina, Chengdu, China

Chong Liang, Research Institute of Petroleum Exploration and Development, CNPC, Beijing, China

**Abstract:** Supercritical carbon dioxide (SC-CO<sub>2</sub>) fracturing can form more complex fracture network and avoid reservoir damage, making it a lucrative alternative to hydraulic fracturing in shale gas reservoirs. This study establishes a two-dimensional dynamic filtration model of SC-CO<sub>2</sub> fracturing, which considers stress sensitivity, fluid adsorption, dynamic changes of fluid physical parameters, and coupled fracture propagation. According to the established model, the dynamic filtration of fracture elements and matrix pressure variation in fracture propagation are simulated and analyzed. And the influence of dynamic and static filtration model, constant and variable SC-CO<sub>2</sub> physical parameters, and fluid types in the filtration areas on the calculation results, as well as the effects of stress sensitivity and fluid adsorption on the filtration process are analyzed. The results show that during the fracturing process, fracture elements' average filtration rate gradually drops and finally becomes stable, while the cumulative filtration volume increases nearly linearly. The static filtration model of uncoupled fracture propagation or the simplification of fluid in the filtration areas to SC-CO<sub>2</sub> single phase provides the reduction of calculation results, while constant SC-CO<sub>2</sub> physical parameters or the fluid simplification to the methane (CH<sub>4</sub>) single phase have the opposite effect. Stress sensitivity can accelerate the filtration, while fluid adsorption can slow down the filtration. The influence of stress sensitivity is maximal at the middle stage of fracturing, while the influence of fluid adsorption weakens with time. This study's findings have important guiding significance for the optimal design and field application of SC-CO<sub>2</sub> fracturing in shale gas reservoirs. © 2021 Society of Chemical Industry and John Wiley & Sons, Ltd.

**Keywords:** adsorption; dynamic filtration model; stress sensitivity; supercritical carbon dioxide

## Introduction

Hydraulic fracturing is often used to improve shale gas well production in order to mitigate the low porosity and low permeability of shale

gas reservoirs.<sup>1,2</sup> However, in the presence of abundant clay minerals in the reservoir, the slickwater fracturing fluid causes clay mineral expansion after entering the reservoir, further reducing the reservoir permeability and seriously affecting the gas production.<sup>3,4</sup>

Correspondence to: Liqiang Zhao, State Key Laboratory of Reservoir Geology and Development Engineering, Southwest Petroleum University, Chengdu 610500, China.

E-mail: zhaoliqiangswpu@163.com

Received March 16, 2021; revised May 8, 2021; accepted May 11, 2021

Published online at Wiley Online Library (wileyonlinelibrary.com). DOI: 10.1002/ghg.2097

Compared with hydraulic fracturing technology, anhydrous one has unique advantages in reducing reservoir damage and water resource dependence. Thus, it gradually gets attention.<sup>5–8</sup> Insofar as supercritical carbon dioxide (SC-CO<sub>2</sub>) combines high density, low viscosity, high diffusion coefficient, and low surface tension, some scholars proposed to use SC-CO<sub>2</sub> for fracturing in shale gas reservoirs.<sup>9,10</sup> SC-CO<sub>2</sub> fracturing fluid can reduce reservoir damage and rock breakdown pressure, as well as connect more natural fractures. Moreover, SC-CO<sub>2</sub> can replace methane adsorbed on the rock surface, improve shale gas reservoir recovery, and realize the permanent geological storage of CO<sub>2</sub>.<sup>11–14</sup>

Under the effect of the pressure difference between fracture and matrix, the SC-CO<sub>2</sub> fracturing fluid will gradually filtrate into the matrix. The filtration will affect the total mass of SC-CO<sub>2</sub> fracturing fluid in the fracture, further affecting the fracture morphology and size.<sup>15</sup> Therefore, it is very important to describe the filtration process accurately. At present, there are few numerical and experimental studies on the filtration of SC-CO<sub>2</sub> fracturing fluid. Tudor and Poleschuk<sup>16</sup> conducted a filtration experiment of liquid CO<sub>2</sub>. The experimental results show that the turbulence effect caused by the high-speed flow of CO<sub>2</sub> will produce additional flow resistance, forming a kind of filter cake similar to the water-base fracturing fluid's filtration process. The virtual filter cake will reduce the filtration rate of CO<sub>2</sub>. Moreover, in high-temperature or low-pressure reservoirs, the expansion of CO<sub>2</sub> will further reduce the filtration rate. Ivory *et al.*<sup>17</sup> found that with pressure decline in the filtration process, the gasification and expansion of liquid CO<sub>2</sub> will produce additional resistance, which can reduce the filtration rate of CO<sub>2</sub>, and liquid CO<sub>2</sub> can effectively reduce the water saturation in the core, which is vital for improving the production after fracturing. Ding<sup>18</sup> measured the filtration coefficient of SC-CO<sub>2</sub> fracturing fluid through filtration experiment and analyzed the influence of temperature, pressure, reservoir fluid and other factors on the filtration coefficient, and found that the filtration coefficient of CO<sub>2</sub> could be significantly reduced under the condition of formation saturated with water and oil. Wang *et al.*<sup>19</sup> established a one-dimensional filtration model considering the physical properties of SC-CO<sub>2</sub> fracturing fluid and the adsorption of SC-CO<sub>2</sub> and CH<sub>4</sub>. The model was verified by the filtration experiment with unconventional core, and the influence of

reservoir permeability, SC-CO<sub>2</sub> viscosity, and filtration pressure difference on the filtration was analyzed.

Previous research on the filtration of SC-CO<sub>2</sub> fracturing fluid were static filtration, so the dynamic filtration law in the process of fracture propagation is still not clear. Therefore, a dynamic filtration model coupled with fracture propagation is established for the first time in this research, moreover, stress sensitivity, fluid adsorption, dynamic variation of fluid physical parameters are also considered. Based on the model, the dynamic filtration law of fracture elements and matrix pressure variation are analyzed, and the influence of dynamic and static filtration model, constant and variable SC-CO<sub>2</sub> physical parameters and fluid types in the filtration areas on the calculation results, as well as the effects of stress sensitivity and fluid adsorption on the filtration process are analyzed. This study is the first time to investigate the dynamic filtration law of SC-CO<sub>2</sub> fracturing in shale gas reservoir.

## Mathematical model

### Filtration model

Insofar as SC-CO<sub>2</sub> has the characteristics of low viscosity and easy diffusion, there is no filter cake in the filtration process, and only the intrusion area and reservoir area are in the filtration areas.<sup>19</sup> The filtration model's basic assumptions used in this study are as follows: the fluid seepage conforms to the linear seepage law, and the reservoir rock is slightly compressible. Moreover, under the condition of shale gas reservoir temperature and pressure, SC-CO<sub>2</sub> piston displaces CH<sub>4</sub>.<sup>19</sup> In addition, the filtration model established in this paper does not consider the influence of natural fractures.

The two-dimensional filtration process is shown in Fig. 1.

(1) Seepage equation in the intrusion area

Because SC-CO<sub>2</sub> will adsorb on the rock surface, the continuity equation of SC-CO<sub>2</sub> fracturing fluid flow in the intrusion area can be obtained by combining with the mass conservation principle. The equation is as follows:

$$\frac{\partial \rho}{\partial t} + \nabla (\rho_s v) = 0 \quad (1)$$

where  $\rho$  is the total mass of SC-CO<sub>2</sub> in rock unit volume,  $\rho_s$  is the total mass of SC-CO<sub>2</sub> flowing in rock unit volume, and  $v$  is the seepage velocity.

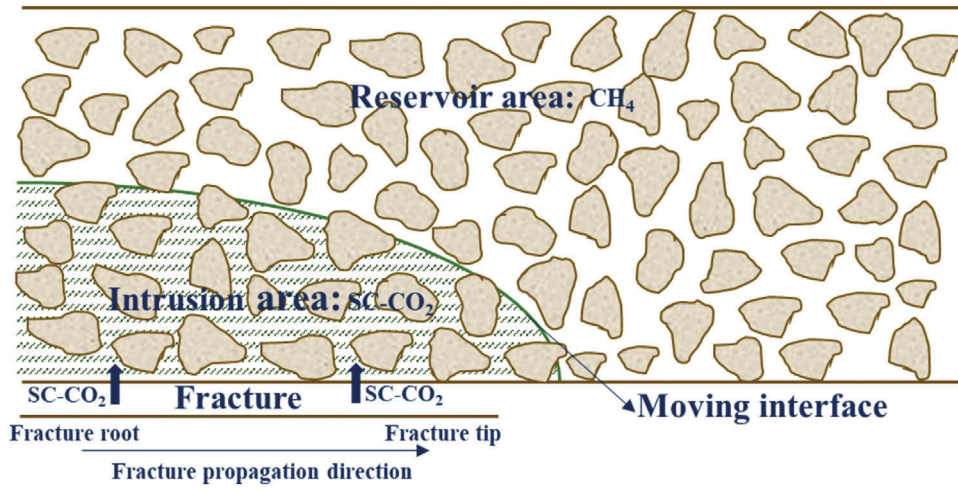


Figure 1. Schematic diagram of the two-dimensional filtration process.

According to the research results of Hu<sup>20</sup>, the adsorption process of SC-CO<sub>2</sub> on shale can be accurately described by the Langmuir adsorption equation:

$$\rho = \phi \rho_s + \rho_{sa} \rho_r V_{sL} \frac{p}{P_{sL} + p} \quad (2)$$

The first term in Eqn (2) is the mass of free SC-CO<sub>2</sub>, while the second term is the mass of adsorbed SC-CO<sub>2</sub>,  $\phi$  is reservoir porosity,  $\rho_{sa}$  is the density of SC-CO<sub>2</sub> in the standard state,  $\rho_r$  is rock density,  $V_{sL}$  is the Langmuir adsorption volume of SC-CO<sub>2</sub>,  $P_{sL}$  is the Langmuir adsorption pressure of SC-CO<sub>2</sub>, and  $p$  is pore pressure.

Given that reservoir rock has certain compressibility, the reservoir rock's porosity state equation should be taken into account:

$$\phi = \phi_0 [1 + C_\phi (p - p_0)] \quad (3)$$

where  $C_\phi$  is the compressibility coefficients of rock, and  $\phi_0$  is the porosity of rock under specific pressure  $p_0$ .

Combining Eqns (2) and (3), the first term of Eqn (1) can be reduced to the following form:

$$\begin{aligned} \frac{\partial \rho}{\partial t} = & \phi_0 (1 - C_\phi p_0) \frac{\partial \rho_s}{\partial t} + \phi_0 C_\phi \frac{\partial (\rho_s p)}{\partial t} \\ & + \rho_{sa} \rho_r V_{sL} \frac{p}{(P_{sL} + p)^2} \frac{\partial p}{\partial t} \end{aligned} \quad (4)$$

Based on the assumption of linear seepage, the motion equation of SC-CO<sub>2</sub> fracturing fluid in the intrusion area is as follows<sup>19</sup>:

$$v = -\frac{k}{\mu_s} \nabla p \quad (5)$$

where  $k$  is the permeability of the reservoir and  $\mu_s$  is the SC-CO<sub>2</sub> viscosity.

Combining Eqns (3) and (5), the second term of Eqn (1) can be reduced to

$$\nabla (\rho_s v) = -\frac{k}{\mu_s} \left[ \frac{\partial}{\partial x} \left( \rho_s \frac{\partial p}{\partial x} \right) + \frac{\partial}{\partial y} \left( \rho_s \frac{\partial p}{\partial y} \right) \right] \quad (6)$$

Combining Eqns (1), (4), and (6), the seepage equation of SC-CO<sub>2</sub> fracturing fluid in the intrusion area can be obtained as follows:

$$\begin{aligned} & \phi_0 (1 - C_\phi p_0) \frac{\partial \rho_s}{\partial t} + \phi_0 C_\phi \frac{\partial (\rho_s p)}{\partial t} \\ & + \rho_{sa} \rho_r V_{sL} \frac{p}{(P_{sL} + p)^2} \frac{\partial p}{\partial t} \\ = & \frac{k}{\mu_s} \left[ \frac{\partial}{\partial x} \left( \rho_s \frac{\partial p}{\partial x} \right) + \frac{\partial}{\partial y} \left( \rho_s \frac{\partial p}{\partial y} \right) \right] \end{aligned} \quad (7)$$

#### (2) Seepage equation in the reservoir area

The adsorption of methane (CH<sub>4</sub>) on shale also satisfies the Langmuir adsorption equation.<sup>20</sup> Similarly, when the Knudsen and slippage effects of CH<sub>4</sub> in the pore flow process are ignored, the seepage equation of

CH<sub>4</sub> in the reservoir area can be obtained:

$$\begin{aligned} & \phi_0 (1 - C_\phi p_0) \frac{\partial \rho_g}{\partial t} + \phi_0 C_\phi \frac{\partial (\rho_g p)}{\partial t} \\ & + \rho_{ga} \rho_r V_{gL} \frac{p}{(P_{sL} + p)^2} \frac{\partial p}{\partial t} \\ & = \frac{k}{\mu_g} \left[ \frac{\partial}{\partial x} \left( \rho_g \frac{\partial p}{\partial x} \right) + \frac{\partial}{\partial y} \left( \rho_g \frac{\partial p}{\partial y} \right) \right] \quad (8) \end{aligned}$$

where  $\rho_{ga}$  is the density of CH<sub>4</sub> in the standard state,  $V_{gL}$  is the Langmuir adsorption volume of CH<sub>4</sub>,  $P_{sL}$  is the Langmuir adsorption pressure of CH<sub>4</sub>, and  $\mu_g$  is the viscosity of CH<sub>4</sub>.

### (3) Stress sensitivity model

Kim *et al.*<sup>21</sup> have revealed the phenomenon of stress sensitivity in shale reservoirs. In this study, the exponential relation is used to calculate the reservoir permeability:

$$k = k_0 \exp(-\beta (\sigma - \sigma_0)) \quad (9)$$

where  $k_0$  is the initial permeability of the reservoir,  $\beta$  is the stress sensitivity coefficient,  $\sigma$  is the effective stress after the pore pressure changes,  $\sigma_0$  is the initial effective stress.

## Fracture propagation model

The filtration model's inner boundary undergoes a dynamic changing process in the actual fracturing process. Thus, the pressure boundary length and boundary values are variable. Therefore, it is necessary to establish a mathematical model of fracture propagation in SC-CO<sub>2</sub> fracturing to obtain the dynamic fracture length and fluid pressure in the fracture to describe the filtration process of SC-CO<sub>2</sub> fracturing fluid more accurately.

### (1) SC-CO<sub>2</sub> fracturing fluid flow equation

Considering the compressibility of SC-CO<sub>2</sub> fracturing fluid and ignoring the change of fracture height, the mass conservation equation in the fracture can be written as follows:

$$\frac{\partial (\rho_f w)}{\partial t} + \frac{\partial (\rho_f q)}{\partial x} + q_L \rho_f = 0 \quad (10)$$

where  $\rho_f$  is the SC-CO<sub>2</sub> fracturing fluid density in the fracture,  $w$  is the fracture width,  $q_L$  is the filtration rate.

The momentum equation of SC-CO<sub>2</sub> fracturing fluid in the fracture can be expressed by classical Poiseuille equation<sup>22</sup>:

$$q = -\frac{w^3}{12\mu_f} \frac{\partial p_f}{\partial x} \quad (11)$$

where  $\mu_f$  is the viscosity of SC-CO<sub>2</sub> fracturing fluid in the fracture,  $p_f$  is the fluid pressure in the fracture.

### (2) Elastic deformation equation

In this study, the semi-analytical and semi-numerical displacement discontinuity method (DDM) is used to describe the elastic deformation of rock. The effect of finite fracture height on the stress and displacement fields is described by the following equilibrium equation<sup>23</sup>:

$$\begin{cases} \sum_{j=1}^N (G^{ij} A_{ss}^{ij} D_s^j + G^{ij} A_{sn}^{ij} D_n^j) = -\frac{1}{2} (\sigma_H - \sigma_h) \sin 2\theta_i \\ \sum_{j=1}^N (G^{ij} A_{ns}^{ij} D_s^j + G^{ij} A_{nn}^{ij} D_n^j) = P_{frc}^i - \sigma_H \sin^2 \theta_i - \sigma_h \cos^2 \theta_i \end{cases} \quad (i, j = 1, 2, \dots, N) \quad (12)$$

where  $A_{ss}^{ij}$ ,  $A_{sn}^{ij}$ ,  $A_{ns}^{ij}$ , and  $A_{nn}^{ij}$  are the influencing coefficients of boundary stress,  $D_s^j$  and  $D_n^j$  are the tangential and normal displacement discontinuities of  $j$ th fracture element, respectively,  $G$  is the three-dimensional correction coefficient,  $\sigma_H$  is the horizontal maximum principal stress in far-field,  $\sigma_h$  is the horizontal minimum principal stress in far-field,  $p_f^i$  is the fluid pressure of  $i$ th fracture element,  $\theta_i$  is the angle between  $i$ th fracture element and the direction of maximum principal stress, and  $N$  is the total number of fracture elements.

## Auxiliary equation

The auxiliary equation is mainly used to calculate the physical parameters of SC-CO<sub>2</sub> and CH<sub>4</sub>. The fracture-matrix temperature field is calculated using the unsteady state model proposed by Sun *et al.*<sup>24</sup> The density, heat capacity, and the Joule-Thomson coefficient of SC-CO<sub>2</sub> are calculated via the Span-Wagner equation<sup>25</sup> The viscosity and thermal conductivity are calculated by the Fenghour-Vesovic model<sup>26,27</sup>. The deviation factor of CH<sub>4</sub> are calculated by the Dranchuk-Abou-Kassem method, and the viscosity is calculated by the Dempsey method.<sup>28</sup> The density of CH<sub>4</sub> is calculated by the state equation of real gas.

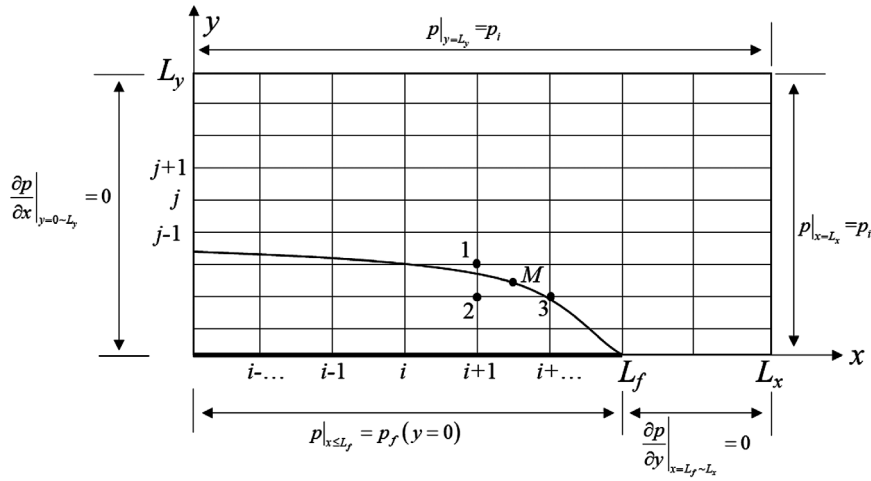


Figure 2. Schematic diagram of fracture and matrix grid.

## Model solution and verification

### Model solution

To reduce computation costs, a grid with the  $x$ -direction coinciding with the fracture propagation direction is constructed for a quarter of the shale gas reservoir, as shown in Fig. 2. The fracture propagation step is equal to the matrix grid length in the  $x$ -direction.

#### (1) Solution conditions

At the initial time, the pore pressures in the intrusion and reservoir areas, as well as at the outer boundary, are equal to the original reservoir pressure  $p_i$ . Meanwhile, the inner boundary pressure in the fracture propagation area is equal to the fluid pressure in the fracture  $p_f$ , whereas that other boundaries are symmetrical. This yields:

$$\begin{cases} p|_{t=0} = p_i \\ p|_{x=L_x} = p|_{y=L_y} = p_i \\ p|_{x \leq L_f} = p_f (y=0) \\ \left. \frac{\partial p}{\partial x} \right|_{x=0, y=0 \sim L_y} = \left. \frac{\partial p}{\partial y} \right|_{x=L_f \sim L_x, y=0} = 0 \end{cases} \quad (13)$$

The fracture initial and tip's current widths are assumed to be zero, the flow rate in the fracture tip is also zero, and the injection displacement is  $q_0$ . Thus, we get

$$\begin{cases} w(s, 0) = 0 \\ w(L_f, t) = 0 \\ q(0, t) = q_0 \\ q(L_f, t) = 0 \end{cases} \quad (14)$$

#### (2) Moving interface

In this study, the moving interface refers to the interface between the intrusion and reservoir areas in the process of piston displacement. And with the continuous filtration of SC-CO<sub>2</sub> fracturing fluid, the interface will continue to move towards the reservoir area. Assuming that the coordinate of each point of the interface at the  $n$ th time step is  $(x_M^n, y_M^n)$ , the expression of each point coordinate under different times can be obtained according to the interface motion speed:

$$\begin{aligned} x_M^{n+1} &= x_M^n + u_M^n \Delta t \\ y_M^{n+1} &= y_M^n + v_M^n \Delta t \end{aligned} \quad (15)$$

where  $x_M^{n+1}$  and  $y_M^{n+1}$  are the abscissa and ordinate of any point  $M$  of the interface at the  $(n+1)$ th time step, respectively;  $x_M^n$  and  $y_M^n$  are the abscissa and ordinate of any point  $M$  of the interface at the  $n$ th time step;  $\Delta t$  is the propagation time step. Finally,  $u_M^n$  and  $v_M^n$  are the extrapolation velocities of the boundary point  $M$  in the  $x$ - and  $y$ -directions at the  $n$ th time step, respectively, which can be derived as follows:

$$\begin{aligned} u_M^n &= \frac{k}{\mu_s(x_{M-1/2}^n)} \left( \frac{p_{x_{M-1}^n}^n - p_{x_M^n}^n}{\Delta x_M} \right) \\ v_M^n &= \frac{k}{\mu_s(x_{M-1/2}^n)} \left( \frac{p_{y_{M-1}^n}^n - p_{y_M^n}^n}{\Delta y_M} \right) \end{aligned} \quad (16)$$

where  $\mu_s(x_{M-1/2}^n)$  is the SC-CO<sub>2</sub> viscosity of the grid with the point  $M$ , while  $p_{x_{M-1}^n}^n$  and  $p_{x_M^n}^n$  are pore pressures in the adjacent nodes of the point  $M$  in the  $x$ -direction

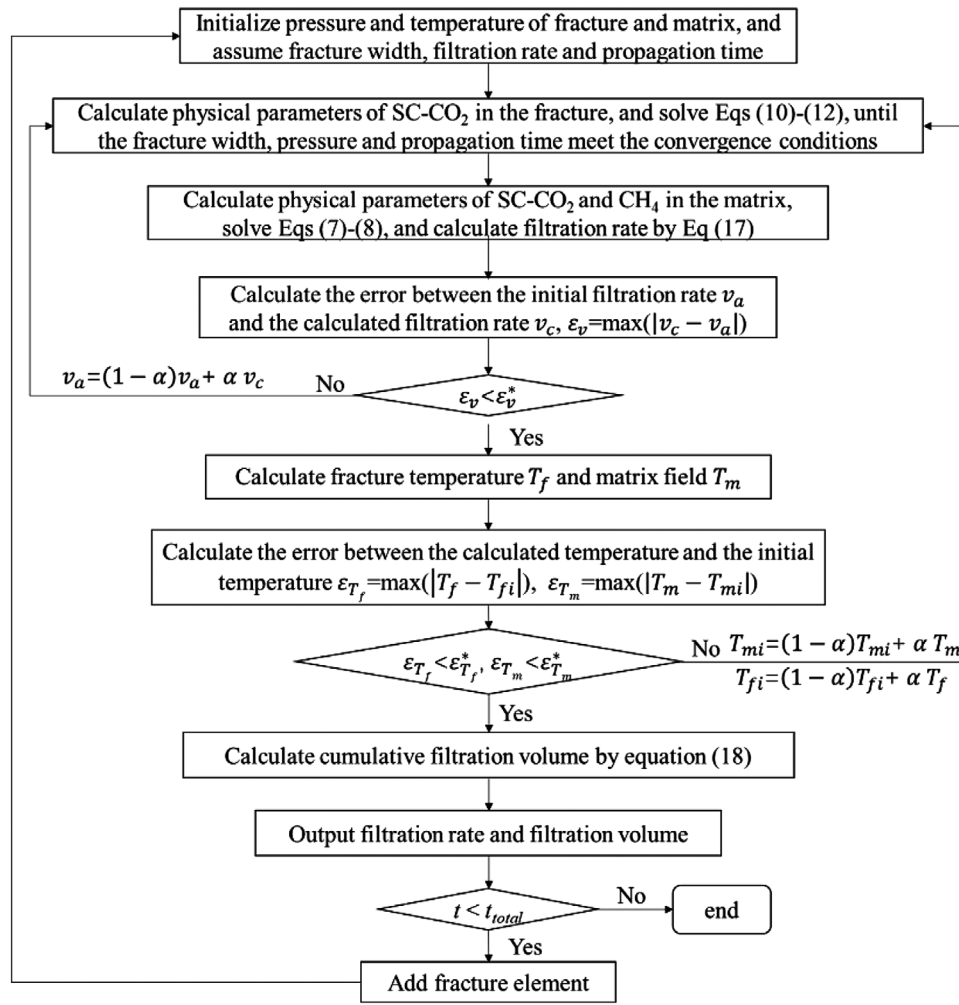


Figure 3. Flowchart of the program design.

(nodes 2 and 3 in Fig. 2). Here  $p_{y_{M-1}}^n$  and  $p_{y_M}^n$  are pore pressures of the adjacent nodes of the point  $M$  in the  $y$ -direction (nodes 1 and 2 in Fig. 2),  $\Delta x_M$  and  $\Delta y_M$  are the grid lengths in the  $x$ - and  $y$ -directions, respectively.

### (3) Coupling solution method

In the SC-CO<sub>2</sub> fracturing fluid filtration law study, the filtration model, fracture propagation model, and temperature field model are involved. In this study, a strong coupling method is used to implement each model. The flowchart of the specific program design is presented in Fig. 3.

Step 1. Initialize fluid pressure in the fracture, pore pressure in the matrix, fracture-matrix temperature field, and assume fracture width, filtration rate, and fracture propagation time.

Step 2. Calculate the physical parameters of SC-CO<sub>2</sub> fracturing fluid in the fracture and carry out iterative

calculation according to the Eqns (10)–(12) until the fracture width, fluid pressure in fracture and propagation time meet the convergence conditions.

Step 3. Calculate the physical parameters of SC-CO<sub>2</sub> in the intrusion area and CH<sub>4</sub> in the reservoir area, take the pressure distribution in the fracture obtained by Step 2 as the inner boundary condition of the filtration model, calculate the pore pressure distribution of the matrix according to the seepage Eqns (7) and (8), and further calculate the filtration rate of each fracture element, and bring in Step 2 to calculate the pressure in the fracture again.

The calculation formula of the filtration rate is as follows:

$$v_{li} = \frac{k}{\mu_{s(1/2)}} \frac{p_{fi}^n - p_{i,1}^n}{\Delta y_1} \quad (17)$$

where  $v_{fi}$  is the filtration rate of  $i$ th fracture element,  $\Delta y_1$  is the first grid length in the  $y$ -direction,  $p_{fi}^n$  is the pressure of  $i$ th fracture element at  $n$ th time step,  $\mu_{s(1/2)}$  is the SC-CO<sub>2</sub> viscosity of adjacent matrix element of  $i$ th fracture element, and  $p_{i,1}^n$  is the pressure of adjacent matrix grid node of  $i$ th fracture element.

Step 4. Repeat Step 2 and Step 3 until the convergence conditions are satisfied.

Step 5. Calculate the fracture–matrix temperature field according to the pressure distribution, filtration rate, and initial temperature distribution.

Step 6. Repeat Step 2–5 until the pressure in the fracture, the pressure in the matrix, and the fracture-matrix temperature field meet the convergence conditions.

Step 7. Output the filtration rate and cumulative filtration volume, in which the calculation formula of cumulative filtration volume is as follows:

$$V_l^n = V_l^{n-1} + 4 \sum_{i=1}^N \frac{k}{\mu_{s(1/2)}} \frac{p_{fi} - p_{i,1}}{\Delta x_i H} \Delta x_i H \quad (18)$$

where  $V_l^n$  and  $V_l^{n-1}$  are the cumulative filtration volume at  $n$ th and  $(n-1)$  th time steps, respectively, and  $\Delta x_i$  are the length of the  $i$ th fracture element.

Step 8. Add fracture element, repeat Step 1–7 until the deadline.

## Model verification

In this section, the established SC-CO<sub>2</sub> fracturing fluid filtration model was verified. Because there is no report on the dynamic filtration model and filtration experiment of coupling fracture propagation, and the two-dimensional dynamic filtration law is quite different from one-dimensional filtration law, the two-dimensional filtration model in this paper was reduced to a one-dimensional model of uncoupled fracture propagation to compare with Wang *et al.*'s model<sup>19</sup> to show the correctness of the filtration model proposed in this paper. Experiments have verified the accuracy of Wang *et al.*'s one-dimensional filtration model.

The values of relevant parameters are as follows: reservoir permeability is  $1.46 \times 10^{-4}$  mD, porosity is 5.72%, the original reservoir pressure is 30 MPa, reservoir temperature is 363 K, SC-CO<sub>2</sub> fluid pressure in the fracture is 35 MPa, the temperature in the fracture is 308 K. The calculation results of the proposed and Wang *et al.*'s model are plotted in Fig. 4.

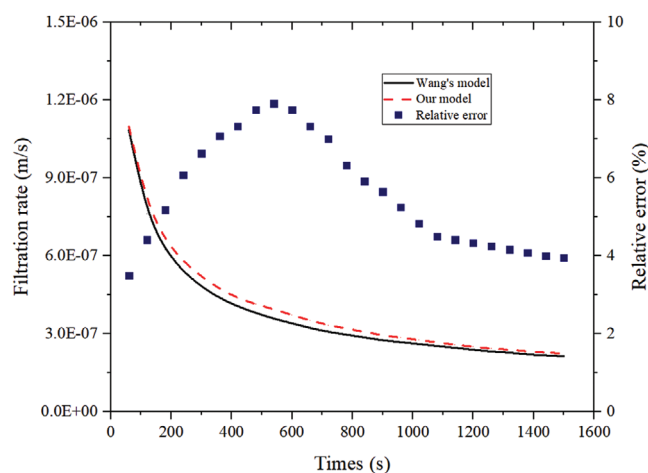


Figure 4. The filtration rate calculated by the proposed and Wang's models.

It can be seen from Fig. 4 that the calculation results of the proposed one-dimensional model reduced from the two-dimensional one are in good agreement with those of Wang *et al.*'s model<sup>19</sup>, and the maximum and average errors are 7.9% and 5.5%, respectively. Part of the calculation results' difference is because the shale gas reservoir's stress sensitivity is considered in our model. The way stress sensitivity affects the filtration rate is analyzed in the next sections.

## Case study

In this section, a case study is analyzed to clarify the dynamic filtration law of SC-CO<sub>2</sub> fracturing fluid. The relevant parameters were obtained from earlier studies<sup>20,29</sup> and summarized in Table 1.

The pressure drop between the fracture element and the adjacent matrix grid node (Fig. 5), the filtration rate of each fracture element (Fig. 6), and the matrix pressure distribution (Fig. 7) are calculated for the grid length in the  $y$ -direction of 0.01 m.

It can be seen from Figs 5–7 that at the initial stage of fracture propagation, the matrix pressure remains unchanged. Still, the pressure in the fracture root is higher than that in the fracture tip. Hence, the fracture element in the fracture root has a larger filtration pressure difference so that the maximum filtration rate is  $8.65 \times 10^{-6} \text{ m s}^{-1}$  in the fracture root. The minimum filtration rate in the fracture tip is  $8.55 \times 10^{-6} \text{ m s}^{-1}$ . Due to the low viscosity of SC-CO<sub>2</sub> fracturing fluid, the difference of fluid pressure in the fracture is small, hence the difference of filtration rates in fracture root and tip is also small at the initial stage.

**Table 1. Parameter values of example analysis.**

| Parameter                             | Value                                   | Parameter                               | Value                                     |
|---------------------------------------|---|---|---|
| Reservoir thickness                   | 30 m                                    | Rock density                            | 2600 kg m <sup>-3</sup>                   |
| Elastic modulus                       | 25 GPa                                  | Poisson's ratio                         | 0.2                                       |
| Original reservoir pressure           | 20 MPa                                  | Original reservoir temperature          | 60 °C                                     |
| Matrix porosity                       | 0.05                                    | Matrix permeability                     | 0.001 mD                                  |
| Horizontal maximum principal stress   | 40 MPa                                  | Horizontal minimum principal stress     | 36 MPa                                    |
| Langmuir volume (CH <sub>4</sub> )    | 2.8 m <sup>3</sup> kg <sup>-1</sup>     | Langmuir pressure (CH <sub>4</sub> )    | 3.5 MPa                                   |
| Langmuir volume (SC-CO <sub>2</sub> ) | 2.1 m <sup>3</sup> kg <sup>-1</sup>     | Langmuir pressure (SC-CO <sub>2</sub> ) | 5.1 MPa                                   |
| Injection displacement                | 3m <sup>3</sup> min <sup>-1</sup>       | Bottom hole temperature                 | 30 °C                                     |
| Stress sensitivity coefficient        | 5 × 10 <sup>-3</sup> M Pa <sup>-1</sup> | Rock compressibility coefficient        | 4.5 × 10 <sup>-4</sup> M Pa <sup>-1</sup> |

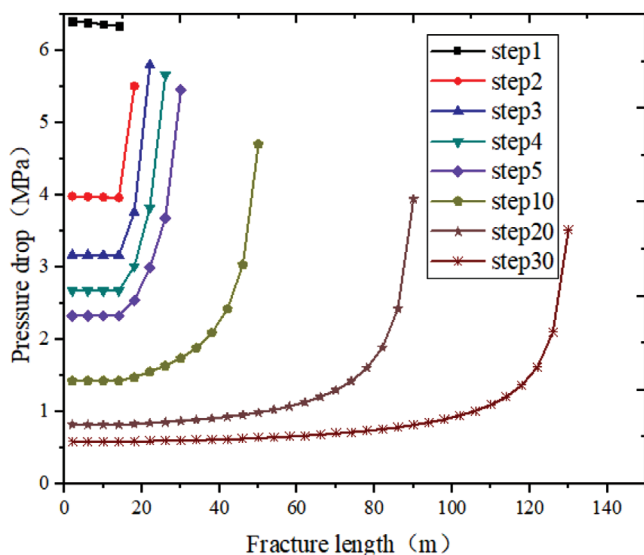


Figure 5. The pressure drop between the fracture element and the adjacent matrix grid node.

With an increase in fracture length, the fracture's fluid continuously filtrates to the matrix and increases the matrix pressure near the nontip fracture elements. However, the pressure difference between the fracture element in the fracture tip and matrix is the difference between the minimum principal stress and the reservoir pressure, so the maximum filtration rate of the fracture element in the fracture tip is  $5.51 \times 10^{-6} \text{ m s}^{-1}$ , and the minimum filtration rate of the adjacent fracture element is  $3.96 \times 10^{-6} \text{ m s}^{-1}$ . When the fracture length is large enough, the pressure in matrix elements along the fracture propagation direction decreases gradually. Hence, the pressure drop between the fracture and matrix elements increases gradually. Finally, the filtration rate is the lowest in the fracture

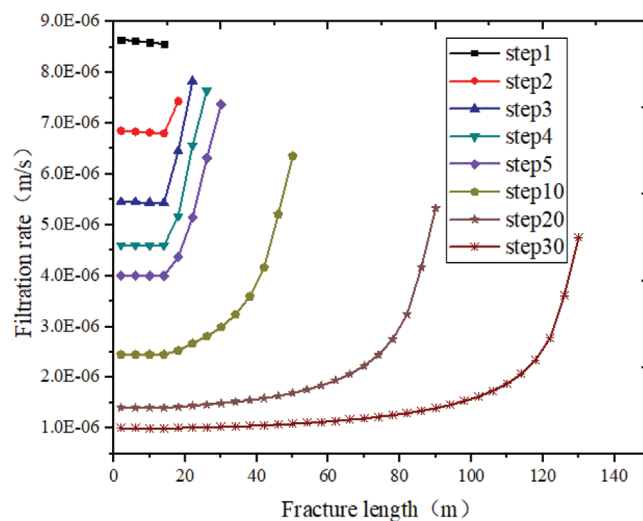


Figure 6. Filtration rate of each fracture element under different propagation time steps.

root, increases sharply near the fracture tip, reaching its maximum in the fracture tip.

Due to the expansion effect of SC-CO<sub>2</sub> and the decrease of filtration pressure difference caused by the increase of matrix pressure, each fracture element's filtration rate is gradually decreasing. Although SC-CO<sub>2</sub> fracturing fluid's viscosity is low and easy to filtrate, SC-CO<sub>2</sub> fracturing fluid's intrusion area is still small. The propagation range of pressure waves is limited because the reservoir is relatively tight (Fig. 7).

To analyze the overall filtration evolution pattern, the average filtration rate is obtained by averaging those of all fracture elements, and the cumulative filtration volume at different times is calculated via Eqn (18).

It can be seen from Fig. 8 that the maximum average filtration rate of all fracture elements is  $8.6 \times 10^{-6} \text{ m}$

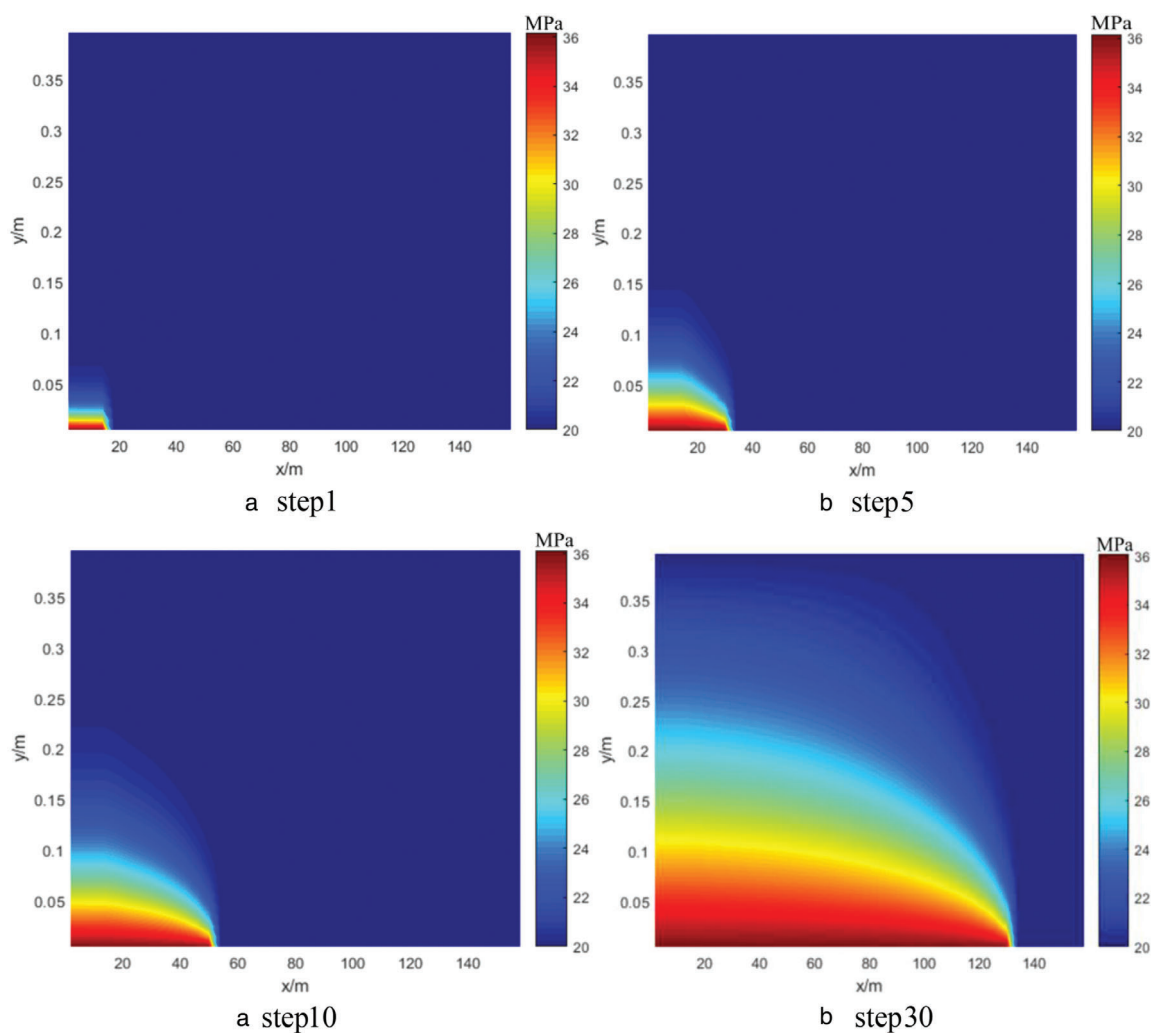


Figure 7. Pore pressure distribution of matrix under different propagation time steps.

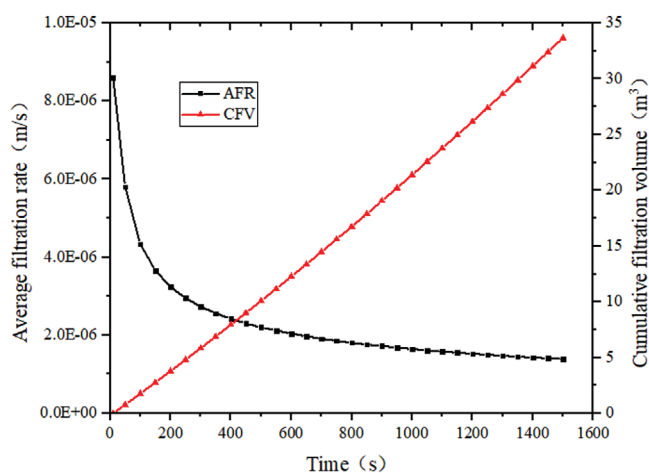


Figure 8. Average filtration rate and cumulative filtration volume at different times, where AFR is an average filtration rate, and CFV is cumulative filtration volume.

$s^{-1}$  at the initial stage of fracturing. At the later stage of fracturing, even if the fracture element in the fracture tip has a larger filtration rate, that of most fracture elements is relatively low, so that the average filtration rate is still low. Finally, the average filtration rate is stable at about  $1.4 \times 10^{-6} \text{ m/s}^{-1}$ . At the early stage of fracturing, the average filtration rate is high, and there are few fracture elements. At the later stage of fracturing, the average filtration rate is low, and there are many fracture elements. Therefore, the cumulative filtration volume increases linearly, and the growth rate is slightly accelerated at the later stage of fracturing.

## Discussion

In this section, the effects of dynamic and static filtration model, constant and variable SC-CO<sub>2</sub>

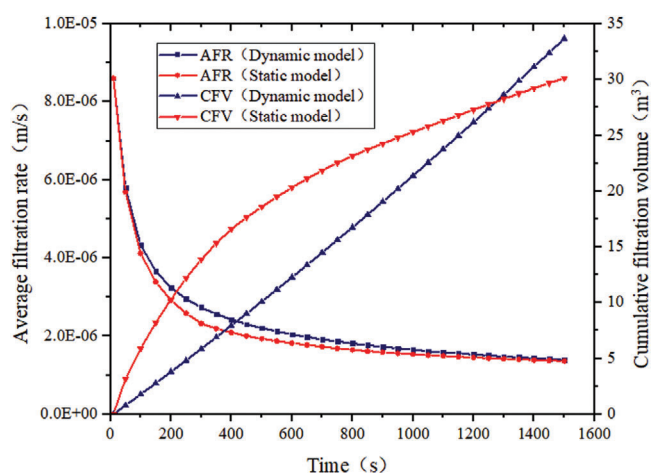


Figure 9. Evolutions of the average filtration rate and cumulative filtration volume calculated for dynamic and static filtration models.

physical parameters and fluid types in the filtration areas on the calculation results, as well as the effects of stress sensitivity and fluid adsorption on the filtration process, are analyzed.

### Dynamic and static filtration model

The difference between dynamic filtration and static filtration mentioned in this study is that the former needs to consider fracture propagation, while the latter does not. The average filtration rate and cumulative filtration volume of them are calculated as follows:

1. According to the method of model solution section, considering the fracture propagation, the fracture length  $L_f$  at a given time  $t_f$ , the dynamic average filtration rate  $v_d$  and dynamic cumulative filtration volume  $V_d$  can be calculated.
2. Without considering the fracture propagation, the final fracture length  $L_f$  is preset first. And the boundary value within the fracture length  $L_f$  is the fluid pressure in the fracture calculated from dynamic filtration. The static average filtration rate  $v_s$  and static cumulative filtration volume  $V_s$  also can be calculated under the condition of constant fracture length  $L_f$ .

The calculation results are plotted in Fig. 9.

It can be seen from Fig. 9 that, compared with the dynamic filtration model coupled with fracture propagation, the average filtration rate calculated by the static filtration model has little difference at the early and late fracturing stages, while the maximum difference at the middle fracturing stage is  $0.41 \times$

$10^{-6} \text{ m s}^{-1}$ . The average filtration rate at all fracturing times calculated by the static model is lower by  $0.17 \times 10^{-6} \text{ m s}^{-1}$  than that calculated by the dynamic model. The reason is that at the early stage of fracturing, the filtration pressure difference in the static and dynamic models is equal, so the average filtration rate is equal, but in the static model, the filtration boundary is longer. There are more fracture elements, so the cumulative filtration volume increases faster. With time, the filtration pressure difference at the static model's filtration boundary decreases continuously. The filtration pressure difference of some fracture elements in the dynamic model decreases gradually. In contrast, the newly added fracture elements still maintain a larger filtration pressure difference after propagation, so the average filtration rate calculated by the static model is lower. The cumulative filtration volume is higher because of the long filtration boundary in the static model, but this increase gets smaller. At the later stage of fracturing, the average filtration rate and cumulative filtration volume tend to be stable due to the constant filtration boundary and stable matrix pressure near the fracture in the static model. In the dynamic model, although the filtration rate of newly added fracture elements is higher, most fracture elements' filtration rates, as well as the average value, tend to be stable. As the fracture length keeps increasing, so does the cumulative filtration volume. The dynamic model's cumulative filtration volume exceeds that of the static model by  $3.54 \text{ m}^3$  because the dynamic model has added fracture elements, which promotes the pressure wave transfer, thus speeding up the fluid filtration.

### Constant and variable SC-CO<sub>2</sub> physical parameters

When calculating the filtration rate of SC-CO<sub>2</sub> fracturing fluid, to reduce the calculation workload, the physical parameters of SC-CO<sub>2</sub> are often treated as fixed values. Therefore, the influence of constant and variable physical parameters of SC-CO<sub>2</sub> (mainly density and viscosity) on the calculation results is analyzed. Without considering the variation of SC-CO<sub>2</sub> physical parameters, their temperature and pressure are the reservoir temperature  $T_r$  and the average value  $P_a$  of the horizontal minimum principal stress and reservoir pressure, respectively. The above temperature and pressure data are easier to obtain. The calculation results are plotted in Fig. 10.

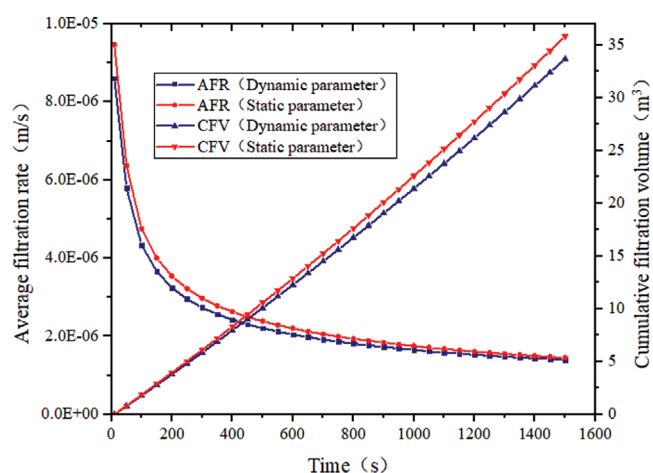


Figure 10. Evolutions of the average filtration rate and cumulative filtration volume calculated for constant and dynamic physical parameters.

It can be seen from Fig. 10 that the average filtration rate calculated using constant physical parameters is higher than that calculated with dynamic parameters, and the maximum difference at the initial stage of fracturing is  $0.86 \times 10^{-6} \text{ m s}^{-1}$ . With time, the difference between constant and dynamic predictions gradually decreases. The average filtration rate and cumulative filtration volume calculated with constant physical parameters exceed dynamic estimations by  $0.18 \times 10^{-6} \text{ m s}^{-1}$  and  $2.15 \text{ m}^3$ , respectively. The reason is that the SC-CO<sub>2</sub> fracturing fluid temperature is lower than the reservoir temperature  $T_r$ , while the pressure exceeds the average pressure  $P_a$  at the initial stage of fracturing. Thus, the SC-CO<sub>2</sub> temperature will be overestimated, and the SC-CO<sub>2</sub> pressure will be underestimated in the calculation process via constant physical parameters. In the supercritical region, the temperature increase and pressure drop will decrease the SC-CO<sub>2</sub> viscosity and accelerate the filtration. Therefore, the predictions via constant physical parameters are overestimated. With time, the SC-CO<sub>2</sub> temperature in the intrusion area gradually grows, and temperature difference with the reservoir drops. At the same time, the pressure waves gradually propagate to the reservoir area so that the SC-CO<sub>2</sub> average pressure in the intrusion area gradually approaches pressure  $P_a$ , so the difference of filtration rates calculated with constant and variable parameters gradually drops. Moreover, constant physical parameters cannot reflect the additional filtration resistance caused by the SC-CO<sub>2</sub> expansion with temperature increase and

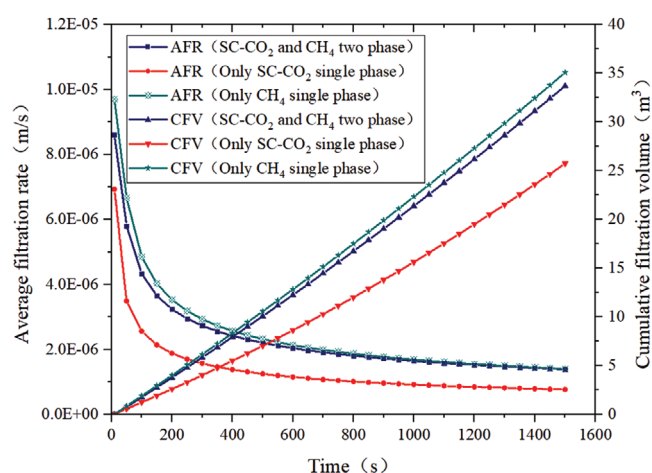


Figure 11. Evolutions of the average filtration rate and cumulative filtration volume calculated for various fluid types.

pressure drop, so the calculation results on filtration rates will be overestimated.

### Fluid types in the filtration areas

The fluid in the filtration areas is usually treated as SC-CO<sub>2</sub> single-phase or CH<sub>4</sub> single phase to simplify the calculation. This simplification will bring errors in the calculation results. Therefore, the effect of fluid type in the filtration areas on the calculation results was analyzed. The average filtration rate and cumulative filtration volume evolutions for various fluid types are plotted in Fig. 11.

In the case of CH<sub>4</sub> single-phase fluid in the filtration areas, the pressure wave propagates slower due to the large compressibility of CH<sub>4</sub>, which leads to a larger filtration pressure difference at the same filtration time. Due to the larger filtration pressure difference and lower CH<sub>4</sub> viscosity, the initial average filtration rate is  $9.6 \times 10^{-6} \text{ m s}^{-1}$ , which exceeds the two-phase case by  $0.99 \times 10^{-6} \text{ m s}^{-1}$ . With time, this difference drops gradually and finally tends to zero. Still, the final cumulative filtration volume in the CH<sub>4</sub> single-phase case exceed the two-phase ones by  $1.39 \text{ m}^3$ .

In the case of SC-CO<sub>2</sub> single-phase fluid in the filtration areas, the initial average filtration rate is  $6.9 \times 10^{-6} \text{ m s}^{-1}$ , which is lower by  $1.68 \times 10^{-6} \text{ m s}^{-1}$  than the two-phase one. With time, this difference firstly increases and then decreases, but the absolute difference is still large. The average filtration rate at all fracturing times and final cumulative filtration volume in the SC-CO<sub>2</sub> single-phase case are lower by  $0.96 \times$

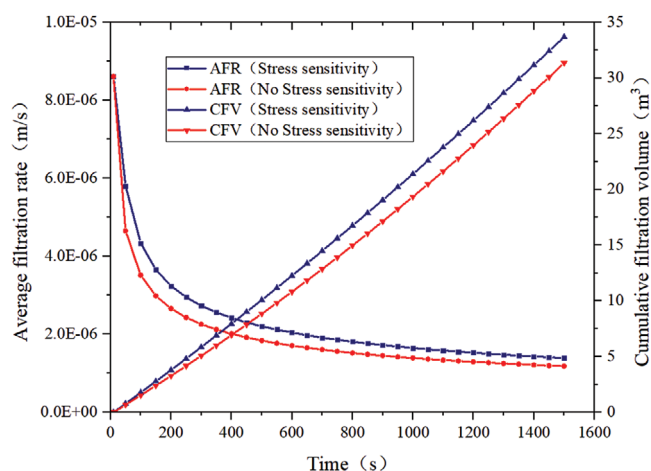


Figure 12. Evolutions of the average filtration rate and cumulative filtration volume with account and disregard of stress sensitivity.

$10^{-6}$  m/s and  $7.95$  m<sup>3</sup> than the two-phase ones. The reason is that less fluid enters the matrix at the initial stage of fracturing in both two-phase and single-phase cases, which have little effect on reservoir pressure and calculation results. With time, the pressure difference between fracture and matrix is smaller due to the lower SC-CO<sub>2</sub> compressibility and faster propagation of pressure waves. Higher viscosity and smaller filtration pressure difference of SC-CO<sub>2</sub> jointly reduce the filtration rate and increase calculation error. At the later stage of fracturing, the matrix pressure and filtration pressure difference gradually stabilize. Therefore, the error induced via matrix fluid simplification by an SC-CO<sub>2</sub> single phase is gradually reduced.

### Stress sensitivity

There is a certain stress sensitivity in shale gas reservoirs, which effect on filtration rate is analyzed in this section. The average filtration rates and cumulative filtration volumes with and without the account of stress sensitivity are plotted in Fig. 12. It can be seen from Fig. 12 that at the start of the fracturing process, the stress sensitivity has little effect on the filtration rate: the average value is  $8.6 \times 10^{-6}$  m s<sup>-1</sup> with and without this effect account. The amount of SC-CO<sub>2</sub> fracturing fluid entering the matrix at the initial stage is small; the respective matrix pore pressure variation is low, so the stress sensitivity is negligible. With time, the amount of SC-CO<sub>2</sub> fracturing fluid entering the matrix increases, the matrix pore pressure variation is large, and the stress sensitivity is pronounced. The highest average filtration rate calculated with an account of

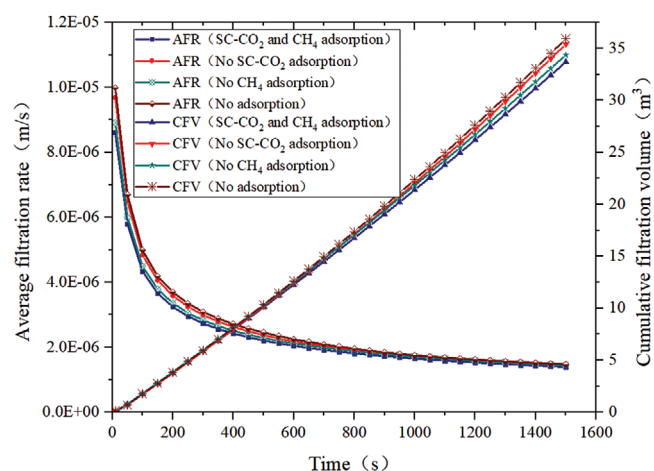


Figure 13. Evolutions of the average filtration rate and cumulative filtration volume with account and disregard of fluid adsorption.

stress sensitivity exceeds that with no account by  $1.2 \times 10^{-6}$  m s<sup>-1</sup>. At the later fracture stage, due to a small pressure difference between fracture and matrix, the stress sensitivity only affects the matrix elements near the fracture tip and, thus, is negligible. Since the average filtration rates calculated with the account of stress sensitivity always exceed those neglecting this effect, this trend is also followed by the cumulative filtration volume. As the above difference grows at the later fracturing stage, the cumulative filtration volumes' difference reaches  $2.35$  m<sup>3</sup>. Therefore, the one-dimensional filtration rates calculated by the proposed model with the account of stress sensitivity systematically exceed Wang *et al.*'s model predictions<sup>19</sup>.

### Fluid adsorption

In contrast to conventional reservoirs, SC-CO<sub>2</sub> or CH<sub>4</sub> in shale gas reservoirs have a certain adsorption capacity. The latter affects the propagation of pressure waves and further filtration rate of SC-CO<sub>2</sub> fracturing fluid. Therefore, this section analyzes the fluid adsorption effect on the filtration process. The latter effects on the average filtration rate and cumulative filtration volume are illustrated in Fig. 13.

It can be seen from Fig. 13 that the initial filtration rate of fracturing in disregard of the SC-CO<sub>2</sub> adsorption is  $9.68 \times 10^{-6}$  m s<sup>-1</sup>, which is higher by  $1.08 \times 10^{-6}$  m s<sup>-1</sup> than that calculated for two-phase adsorption. This difference gradually drops and tends to be stable with time. This trend can be attributed to the lack of SC-CO<sub>2</sub> adsorption on the rock at the initial

stage of fracturing, and the rapid adsorption of SC-CO<sub>2</sub> can reduce the pore radius of the matrix, which prevents SC-CO<sub>2</sub> in the fracture from entering the pores, so the adsorption has a great influence on the filtration rate at the initial stage of fracturing and the filtration rate will be higher when the adsorption is neglected. With time, the adsorption of SC-CO<sub>2</sub> by the rock gradually reaches saturation, so this effect on the filtration rate gradually weakens. At the later stage of fracturing, the pressure difference between most fracture elements and matrix elements is stable, and the filtration rate is low. Even if SC-CO<sub>2</sub> adsorption strongly affects the matrix elements near the fracture tip, the average filtration rate's effect is still weak, and the final calculation results with SC-CO<sub>2</sub> adsorption account or disregard tend to be consistent. When CH<sub>4</sub> adsorption is neglected, the average filtration rate exhibits a slight increase of  $0.06 \times 10^{-6} \text{ m s}^{-1}$  at all fracturing times. On the one hand, the adsorption capacity of CH<sub>4</sub> is weaker than that of SC-CO<sub>2</sub>. On the other hand, the pressure of the matrix containing CH<sub>4</sub> is lower. The combined effect of these two factors results in that the adsorption of CH<sub>4</sub> has little effect on the filtration rate. When the adsorption of SC-CO<sub>2</sub> and CH<sub>4</sub> is neglected, the filtration rate is further increased due to both factors' superposition effect.

## Conclusions

In this study, a two-dimensional dynamic filtration model considering stress sensitivity, fluid adsorption, dynamic changes of fluid physical parameters, and coupled fracture propagation is established. According to the established model, the dynamic filtration of fracture elements and matrix pressure variation in the process of fracture propagation are simulated and analyzed in detail. The calculated results of average filtration rate and cumulative filtration volume are affected by dynamic and static filtration model, constant and variable SC-CO<sub>2</sub> physical parameters, and fluid types in the filtration area. The stress sensitivity and fluid adsorption effects on the filtration process are also clarified. The results obtained made it possible to draw the following conclusions.

- At the initial stage of SC-CO<sub>2</sub> fracturing, the filtration rate of the fracture element in the fracture root is the highest and gradually changes to that in the fracture tip with time. And the average filtration rate at the initial stage reaches its maximum, then

gradually drops, and finally stabilizes, while the cumulative filtration volume increases nearly linearly.

- The average filtration rate predicted by the static filtration model with uncoupled fracture propagation is higher than that of the dynamic filtration model, while the cumulative filtration volume increases faster at the initial stage, slows down with time, and finally becomes lower than that predicted by the dynamic filtration model. The average filtration rate and cumulative filtration volume calculated using constant SC-CO<sub>2</sub> physical parameters are higher than those with dynamic ones due to overestimation of temperature, underestimation of pressure, and failure to consider the additional resistance caused by SC-CO<sub>2</sub> expansion. Simplifying the fluid in the filtration areas to SC-CO<sub>2</sub> single phase will result in lower calculation results, while simplifying the fluid in the filtration areas to CH<sub>4</sub> single phase will result in higher calculation results.
- Stress sensitivity can accelerate the filtration of SC-CO<sub>2</sub> fracturing fluid, and the influence of stress sensitivity on the filtration rate reaches its maximum at the middle stage of fracturing, being negligible at the early and late stages. However, fluid adsorption can slow down the filtration of SC-CO<sub>2</sub> fracturing fluid, and the influence of fluid adsorption decays with time, and the influence of SC-CO<sub>2</sub> adsorption on filtration is stronger than that of CH<sub>4</sub>.

## Nomenclature

|  |   |
|--|---|
| $A_{ss}^{ij}, A_{sn}^{ij}, A_{ns}^{ij}, A_{nm}^{ij}$ | Influence coefficients of boundary stress, Pa <sup>-1</sup> |
| $C_\phi$   | Compressibility coefficient of rock, Pa <sup>-1</sup>       |
| $D_s^j$  | Tangential displacement discontinuity of $j$ th element, m  |
| $D_n^j$  | Normal displacement discontinuity of $j$ th element, m      |
| $G$  | Three-dimensional correction factor, dimensionless          |
| $H$  | Fracture height, m  |
| $k$  | Permeability of the reservoir, m <sup>2</sup>               |
| $k_0$  | The initial permeability of the reservoir, m <sup>2</sup>   |
| $L_f$  | Fracture length, m  |
| $N$  | Total number of fracture elements                           |
| $p$  | Pore pressure, Pa   |

|              |   |
|--------------|---|
| $p_f$        | Fluid pressure in fracture, Pa  |
| $p_f^i$      | Fluid pressure in $i$ fracture element, Pa  |
| $P_{sL}$     | Langmuir adsorption pressure of SC-CO <sub>2</sub> , Pa   |
| $P_{gL}$     | Langmuir adsorption pressure of CH <sub>4</sub> , Pa  |
| $q_L$        | Filtration rate, m s <sup>-1</sup>  |
| $q_0$        | Injection displacement, m <sup>3</sup> s <sup>-1</sup>  |
| $V_l^n$      | Cumulative filtration volume at $n$ th time step, m <sup>3</sup>                                    |
| $V_{sL}$     | Langmuir adsorption volume of SC-CO <sub>2</sub> , m <sup>3</sup> kg <sup>-1</sup>                  |
| $V_{gL}$     | Langmuir adsorption volume of CH <sub>4</sub> , m <sup>3</sup> kg <sup>-1</sup>                     |
| $w$          | Fracture width, m   |
| $\beta$      | Stress sensitivity coefficient, Pa <sup>-1</sup>  |
| $\Delta x_i$ | The length of $i$ th fracture element, m  |
| $\theta_i$   | The angle between $i$ th fracture element and direction of horizontal maximum principal stress, rad |
| $\mu_s$      | Viscosity of SC-CO <sub>2</sub> , Pa s <sup>-1</sup>  |
| $\mu_g$      | Viscosity of CH <sub>4</sub> , Pa s <sup>-1</sup>   |
| $\mu_f$      | Viscosity of SC-CO <sub>2</sub> fracturing fluid in fracture, Pa s <sup>-1</sup>                    |
| $v$          | Seepage velocity, m s <sup>-1</sup>   |
| $v_{ii}$     | Filtration rate of $i$ th fracture element, m s <sup>-1</sup>                                       |
| $\rho$       | SC-CO <sub>2</sub> density (mass of SC-CO <sub>2</sub> per rock unit volume), kg m <sup>-3</sup>    |
| $\rho_f$     | Density of SC-CO <sub>2</sub> fracturing fluid in fracture, kg m <sup>-3</sup>                      |
| $\rho_{ga}$  | Density of CH <sub>4</sub> in the standard state, kg m <sup>-3</sup>                                |
| $\rho_r$     | Rock density, kg m <sup>-3</sup>  |
| $\rho_s$     | The total mass of SC-CO <sub>2</sub> flowing in rock unit volume, kg m <sup>-3</sup>                |
| $\rho_{sa}$  | Density of SC-CO <sub>2</sub> in the standard state, kg m <sup>-3</sup>                             |
| $\sigma$     | Effective stress after pore pressure change, Pa   |
| $\sigma_0$   | Initial effective stress, Pa  |
| $\sigma_H$   | Horizontal maximum principal stress in far-field, Pa  |
| $\sigma_h$   | Horizontal minimum principal stress in far-field, Pa  |
| $\phi$       | Reservoir porosity, dimensionless   |
| $\phi_0$     | Rock porosity at a specific pressure $p_0$ , dimensionless  |

## Acknowledgements

This work was supported by the National Natural Science Foundation of China (51974264).

## Conflict of Interest

The authors declare that they have no known competing financial interests or personal relationships that could have appeared to influence the work reported in this paper.

## References

- Zhang F and Emami-Meybodi H, Analysis of early-time production data from multi-fractured shale gas wells by considering multiple transport mechanisms through nanopores. *J Pet Sci Eng* **197** (2021). <https://doi.org/10.1016/j.petrol.2020.108092>
- Zhao Y, Lu G, Zhang L, Wei Y, Guo J and Chang C, Numerical simulation of shale gas reservoirs considering discrete fracture network using a coupled multiple transport mechanisms and geomechanics model. *J Pet Sci Eng* **195** (2020). <https://doi.org/10.1016/j.petrol.2020.107588>
- Le MT, An assessment of the potential for the development of the shale gas industry in countries outside of North America. *Heliyon* **4**(2) (2018).
- Lei H, Baojiang S, Yun L, Qingjie D and Linlin Y, Impact of unconventional oil and gas exploitation on fracturing equipment and materials development. *Nat Gas Ind* **33**(12):105–110 (2013).
- Huang X, Li T, Hu W, Lin H and Yan R, LPG fracturing technology and its prospect on shale gas exploitation in China. *Paper presented at 2015 International Conference on Science and Environment, Rhodes, Greece.* (2015),
- Li G, Wang H, Shen Z, Tian S, Huang Z and Cheng Y, Application investigations and prospects of supercritical carbon dioxide jet in petroleum engineering. *Journal of China University of Petroleum (Edition of Natural Science)* **37**(05):76–80 +87 (2013).
- Wen H, Yang R, Huang Z, Zheng Y, Wu X and Hu X, Numerical simulation of proppant transport in liquid nitrogen fracturing. *Journal of Natural Gas Science and Engineering* **84**:(2020). <https://doi.org/10.1016/j.jngse.2020.103657>
- Zhao J, Chen P, Liu Y and Mao J, Development of an LPG fracturing fluid with improved temperature stability. *J Pet Sci Eng* **162**:548–553 (2018).
- He Z, Tian S, Li G, Wang H, Shen Z and Xu Z, The pressurization effect of jet fracturing using supercritical carbon dioxide. *Journal of Natural Gas Science and Engineering* **27**:842–851 (2015).
- Wang H, Li G, Shen Z, Tian S, Sun B, He Z and Lu P, Experiment on rock breaking with supercritical carbon dioxide jet. *J Pet Sci Eng* **127**:305–310 (2015).
- Jiang Y, Qin C, Kang Z, Zhou J, Li Y, Liu H and Song X, Experimental study of supercritical CO<sub>2</sub> fracturing on initiation pressure and fracture propagation in shale under different triaxial stress conditions. *Journal of Natural Gas Science and Engineering* **55**:382–394 (2018).

12. Wang L, Yao B, Xie H, Kneafsey TJ, Winterfeld, PH., Yin X and Wu Y, Experimental investigation of injection-induced fracturing during supercritical CO<sub>2</sub> sequestration. *International Journal of Greenhouse Gas Control* **63**:107–117 (2017).
13. Zhang Y, Zhang Z, Sarmadivaleh M, Lebedev M, Barifcani A, Yu H and Iglaier S, Micro-scale fracturing mechanisms in coal induced by adsorption of supercritical CO<sub>2</sub>. *International Journal of Coal Geology* **175**:40–50 (2017).
14. Zhou D, Zhang G, Wang Y and Xing Y, Experimental investigation on fracture propagation modes in supercritical carbon dioxide fracturing using acoustic emission monitoring. *International Journal of Rock Mechanics and Mining Sciences* **110**:111–119 (2018).
15. Meng Y, Li Z and Lai F, Evaluating the filtration property of fracturing fluid and fracture conductivity of coalbed methane wells considering the stress-sensitivity effects. *Journal of Natural Gas Science and Engineering* **80** (2020). <https://doi.org/10.1016/j.jngse.2020.103379>
16. Tudor R and Poleschuk A, Low-viscosity low-temperature fracture fluids. *Journal of Canadian Petroleum Technology* **35**(07):31–36 (1996).
17. Ivory J, Meier P, De Rocco, M and Scott K, Field and laboratory measurements of leakoff parameters for liquid CO<sub>2</sub> and liquid CO<sub>2</sub>/N<sub>2</sub> fracturing. Paper presented at 48th Annual Technical Meeting of The Petroleum Society, Calgary, Alberta, Canada (1997).
18. Ding L, Study on filtration behavior of liquid CO<sub>2</sub> fracturing, Master's Dissertation. China University of Petroleum (2017).
19. Wang J, Sun B, Wang Z and Zhang J, Study on filtration patterns of supercritical CO<sub>2</sub> fracturing in unconventional natural gas reservoirs. *Greenhouse Gases: Science and Technology* **7**(6):1126–1140 (2017).
20. Hu N, Adsorption characteristics of supercritical CO<sub>2</sub> and CH<sub>4</sub> in Shale Chongqing University, Doctoral Dissertation (2018).
21. Kim TH, Lee JH and Lee KS, Integrated reservoir flow and geomechanical model to generate type curves for pressure transient responses of a hydraulically-fractured well in shale gas reservoirs. *J Pet Sci Eng* **146**:457–472 (2016).
22. Wang D, Research on fracture propagation driven by supercritical carbon dioxide in tight sandstone reservoir. China University of Petroleum (Beijing) (2018).
23. Cheng W, Wang R, Jiang G and Xie J. Modelling hydraulic fracturing in a complex-fracture-network reservoir with the DDM and graph theory. *Journal of Natural Gas Science and Engineering* **47**:73–82 (2017).
24. Sun X, Sun B and Wang Z, Fissure temperature field model of supercritical CO<sub>2</sub> fracturing. *Acta Petrolei Sinica* **36**(12):1586–1592 (2015).
25. Span R and Wagner W, A new equation of state for carbon dioxide covering the fluid region from the triple-point temperature to 1100 K at pressures up to 800 MPa. *Journal of Physical & Chemical Reference Data* **25**(6):1509–1596 (1996).
26. Fenghour A, Wakeham WA and Vesovic V, The viscosity of carbon dioxide. *Journal of Physical & Chemical Reference Data* **27**(1):31 (1998).
27. Vesovic V, Wakeham WA, Olchoway GA and Sengers JV, The transport properties of carbon dioxide. *Journal of Physical & Chemical Reference Data* **19**(3):763–808 (1990).
28. Li S, *Natural gas engineering*. 2nd Edition. Petroleum Industry Press, Beijing (2008).
29. Li Z, Xu H and Zhang C, Liquid nitrogen gasification fracturing technology for shale gas development. *J Pet Sci Eng* **138**:253–256 (2016).



**Zhifeng Luo**

Zhifeng Luo is a professor at Southwest Petroleum University, China, focusing on the theory and technology research of oil and gas reservoir stimulation, especially in acid fracturing, hydraulic fracturing, chemical fracturing and supercritical carbon dioxide fracturing.



**Liqiang Zhao**

Liqiang Zhao is a professor at Southwest Petroleum University, China, focusing on the theory and technology research of acid fracturing and chemical fracturing. He has BSc and MSc degrees in Petroleum Engineering from Southwest Petroleum University.



**Lin Wu**

Lin Wu is a Master's candidate at Southwest Petroleum University, China, focusing on supercritical carbon dioxide fracturing in unconventional reservoirs. He has a BSc in Petroleum Engineering from Southwest Petroleum University.



**Nanlin Zhang**

Nanlin Zhang is a PhD candidate at Southwest Petroleum University, China, focusing on the research of fracture propagation in the process of fracturing. He has BSc and MSc degrees in Petroleum Engineering from Southwest Petroleum University.



**Weihua Chen**

Weihua Chen is an engineer in Engineering Technology Research Institute of Petrochina Southwest Oil and Gas Field Company, focusing on reservoir stimulation in tight sand gas reservoirs and carbonate gas reservoirs.



**Chong Liang**

Chong Liang is a senior engineer in China Petroleum Exploration and Development Research Institute. He graduated from Daqing Petroleum Institute and has been engaged in the research on the oil and gas reservoir stimulation.